

Imaginary Magnetic Tweezers for Massively Parallel Surface Adhesion Spectroscopy

Ye Yang,[†] Randall M. Erb,[§] Benjamin J. Wiley,[‡] Stefan Zauscher,[†] and Benjamin B. Yellen^{*,†,||}

[†]Department of Mechanical Engineering and Materials Science and [‡]Department of Chemistry, Duke University, Durham, North Carolina, United States

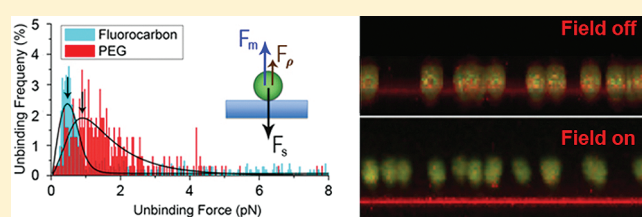
[§]Complex Materials, Department of Materials, ETH-Zürich, 8093 Zürich, Switzerland

^{||}University of Michigan–Shanghai Jiaotong Joint Institute, Shanghai, People's Republic of China

S Supporting Information

ABSTRACT: A massively parallel magnetic tweezer system has been constructed that utilizes the self-repulsion of colloidal beads from a planar interface via a magnetic dipole image force. Self-repulsion enables the application of a uniform magnetic force to thousands of beads simultaneously, which permits the measurement of unbinding histograms at the lowest loading rates ever tested. The adhesion of $9.8\ \mu\text{m}$ polystyrene beads to a fluorocarbon, PEG, and UV-irradiated PEG surfaces were measured between 10^{-3} – 10^0 pN/s force loading rates, revealing the presence of both kinetic and quasi-equilibrium unbinding regimes.

KEYWORDS: Magnetic tweezers, image force, parallel measurements, surface force, quasi-equilibrium, loading rate



Accurate measurement of surface adhesion forces and intermolecular unbinding forces remains a long-standing problem in biophysics and materials science due to the strong influence of thermal noise on the measurement. Typically, a large ensemble of measurements (1000 or more) is required to obtain a statistically reliable measure of the mean unbinding force between a probe (e.g., an atomic force microscopy (AFM) tip or a colloidal bead) and a surface.^{1,2} Most surface force tools, such as those based on AFM,^{3–5} optical tweezers,^{6–8} biomembrane force probe,^{9,10} and surface force apparatus,¹¹ can conduct only one (or a few) unbinding measurement at a time. Furthermore, the mean unbinding force is highly sensitive to the force loading rate, requiring these measurements to be conducted over multiple force loading regimes, which considerably increases the number of experiments required and lengthens the analysis time. Finally, existing techniques are not able to access the extremely low loading rates required to observe the quasi-equilibrium unbinding regime in which unbinding is caused by a combination of random thermal motion and the externally applied mechanical potential.¹²

Magnetic forces are an attractive route for parallelizing surface force measurements because magnetic force can be transmitted to thousands of functionalized colloidal beads simultaneously using a small solenoid or a permanent magnet placed above the substrate.^{13–15} However, the high variability in the magnetic properties of each magnetic bead (typically $\pm 20\%$ for a reasonably monodisperse batch) as well as the presence of nonuniform fields and field gradients at different locations on the substrate, introduces uncertainty and necessitates a tedious calibration procedure for each force measurement. Here, we present an

alternative approach based on the “magnetic image force” between spherical beads and planar substrates, which harnesses the self-repulsion of beads from surfaces to achieve greater uniformity in the applied force. Self-repulsion transmits a highly uniform force to each bead simultaneously and allows for loading rates that can potentially span the range of 10^{-4} – 10^2 pN/s, thus reaching down to the quasi-equilibrium force loading regime where valuable thermodynamic properties of the system can be directly obtained.

The sphere/plane interaction naturally lends itself to a solution by “method of images” in which the reaction field of a planar substrate can be represented as the reflection of the multipole content of the spherical bead.¹⁶ This force is repulsive when the magnetic permeability of the fluid, μ_f , is larger than that of the substrate, μ_s , which is achieved by using a ferrofluid (a dispersion of ~ 10 nm magnetic nanoparticles suspended in an aqueous carrier fluid). A schematic of our measurement approach along with some experimental images is provided in Figure 1.

The effective magnetic dipole moment, \vec{m} , of a nonmagnetic bead with volume V exposed to a uniform external magnetic field, \vec{H} , is a classical magnetostatic problem with a solution given by¹⁶ $\vec{m} = 3V\vec{H}(\mu_0 - \mu_f)/(\mu_0 + 2\mu_f)$. When the bead is nearby a nonmagnetic substrate such as glass, the bead/substrate interaction can be modeled through the method of images as the interaction between a true dipole and an image dipole, whose moment is reduced by the factor $(\mu_f - \mu_0)/(\mu_f + \mu_0)$.¹⁷ Since the image

Received: January 17, 2011

Revised: February 23, 2011

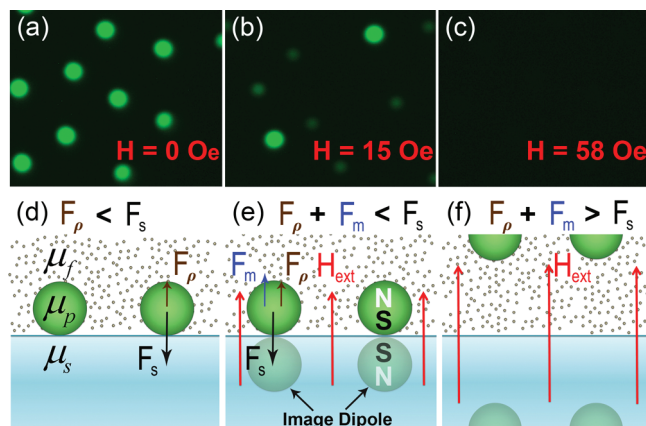


Figure 1. Illustration of surface adhesion analysis using image forces. Images a–c depict 9.8 μm fluorescent beads in the presence of (a) 0, (b) 15, which is near the critical field strength required for unbinding, and (c) 58 Oe uniform magnetic field. In increasing the magnetic field strength, the bead’s fluorescence decays as it is pushed into the ferrofluid via the magnetic image force. The schematic (d–f) illustrates the method for measuring surface forces. In the absence of a magnetic field (d), a bead remains adhered to the substrate surface as the attractive surface forces F_s are stronger than the effective buoyancy force, F_ρ . In a weak magnetic field (e), the magnetic image dipole force F_m adds to the buoyancy force, however the surface force is still stronger ($F_s > F_\rho + F_m$). Above a critical field strength (f), the magnetic repulsion overcomes the surface force ($F_s < F_\rho + F_m$) and the bead is ejected from the substrate.

dipole is always oriented in a repulsive manner to the true dipole regardless of the field orientation, the bead/substrate force is always in the direction of the surface normal, \hat{n} . The bead/substrate interaction is modeled as the force on a point dipole interacting with the field gradient of its own image, that is, $\vec{F}_m = \mu_0(\vec{m} \cdot \nabla)\vec{H}$, leading to the expression

$$\vec{F}_m = \frac{3\pi\mu_0 d^2 \vec{H}^2}{8(1+2\epsilon)^4} \left(\frac{\mu_f - \mu_0}{\mu_f + \mu_0} \right) \left(\frac{\mu_f - \mu_0}{\mu_f + 2\mu_0} \right)^2 \hat{n} \quad (1)$$

where d is the bead diameter, and $\epsilon = \Delta/d$ is the dimensionless bead/substrate separation with Δ being the separation distance between the bead surface and the planar substrate. We show that this force equation is consistent with our experimental measurements of image forces described next.

To demonstrate the image tweezer approach, we used EMG 705 ferrofluid (Ferrotech, Nashua, NH) and monodisperse, nonmagnetic polystyrene colloidal beads (9.8 μm) (Thermo Scientific, Fremont, CA) with a magnetic permeability nearly equal to vacuum, μ_0 , which was adopted so as to eliminate the permeability variation between different beads. The permeability of the ferrofluid was calibrated through confocal microscopy measurements and a theoretical model based on the balance between magnetic and buoyancy forces. To determine the effective buoyancy force, we first measured the density of the beads relative to the ferrofluid by sedimentation analysis. This was achieved by mixing the beads with volume fractions of ferrofluid ranging from 0 to 4% and observing the ferrofluid concentration at which the beads transitioned from sedimentation to buoyancy. The mass density of the ferrofluid was measured with a microbalance, and the density of the ferrofluid at the sink/float transition was determined to be 1.047 g/cm³. For the ferrofluid concentration

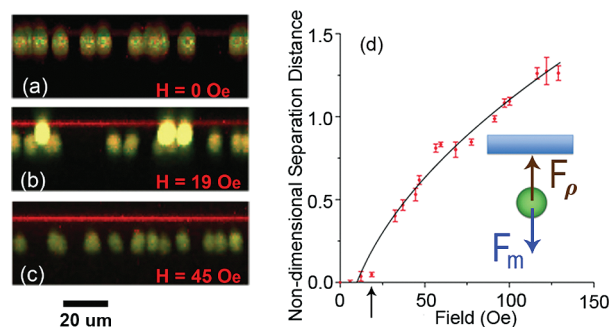


Figure 2. Technique for calibrating magnetic image force. Here, the magnetic image force and buoyancy force are oriented to oppose one another, leading to an equilibrium separation distance that changes as a function of the field strength. Images a–c present confocal microscope images of the bead/substrate separations in uniform external fields of (a) 0, (b) 19, and (c) 45 Oe. The experimental measurements of equilibrium separation distances are provided in (d) along with standard deviations; these values were used to determine the best fit ferrofluid permeability, $\mu_f = 1.66$, from eq 2.

used both in the calibration procedure and surface force analysis, the effective buoyancy force, is calculated to be 0.512 pN based on the relationship, $F_\rho = (\rho_p - \rho_f)Vg$.

When magnetic fields are applied to the colloidal suspension, the image force levitates the beads sufficiently far away from the substrate surface so that the only compensating force remains the effective buoyancy force, with negligible contributions from all other surface forces. In practice, our externally applied field was produced by passing electric current through a solenoid coil (Fischer Scientific) and had a slight field gradient, leading to an additional magnetic force on the bead. This external field induced gradient force was comparable to gravity when high fields in excess of 200 Oe were applied; however for the low fields we typically used in our unbinding experiments the external field induced force (which scales with the square of the external field) was orders of magnitude lower than the gravity and could be ignored both in the calibration steps and the future unbinding experiments.

Thus, by incorporating a force balance, $\vec{F}_m = -\vec{F}_\rho$, an analytical relationship can be derived for the equilibrium bead/substrate separation distance given by

$$\epsilon_{eq} = \frac{1}{2} \left[\sqrt[4]{\frac{9\mu_0 \vec{H}^2}{4dg|\rho_f - \rho_p|} \left(\frac{\mu_f - \mu_0}{\mu_f + \mu_0} \right) \left(\frac{\mu_0 - \mu_f}{\mu_0 + 2\mu_f} \right)^2} - 1 \right] \quad (2)$$

In eq 2 the only free parameter is the ferrofluid permeability, μ_f . This parameter can be experimentally determined by finding the best fit in the ϵ_{eq} versus \vec{H} relationship. Quantitative analysis of bead/substrate separations were obtained directly with a Zeiss LSM 510 upright microscope in external fields ranging from 0 to 150 Oe. Images of the beads show that they are repelled from the glass surface (red line) as the strength of the external field is increased (Figure 2). The match between eq 2 and the experimental data allowed for the determination of the ferrofluid permeability, $\mu_f = 1.66$. The calibration of the ferrofluid permeability is a necessary step due to the potential for particle–particle aggregation and other aging effects that can change the fluid properties over time. However, this result agrees well with the

expected permeability of a quasi-magnetic continuum in the linear regime,¹⁸ which follows the relationship $\mu_f = \mu_0(1 + \phi\mu_0V_f\bar{M}_s^2/3k_B T)$, where V_f is the volume of a typical ferrofluid particle, present at a volume fraction, ϕ , and having saturation magnetization, M_s . Given the following experimental values of $\phi = 3.2\%$, $M_s = 4.84 \times 10^5 \pm 4.7 \times 10^3$ A/m,¹⁹ an effective particle diameter $d = 13.5$ nm would accurately describe the experimentally determined magnetic permeability, which corresponds well with its actual diameter measured in TEM.²⁰ The agreement between theory and experiment is strong when the bead/substrate separation was greater than $1 \mu\text{m}$. At low separations, theory diverged from experiment due to the additional influence of surface forces (e.g., DLVO forces, hydrophobic effects), which were not taken into account in the force balance during calibration. One experimental point denoted by the black arrow in Figure 2d clearly shows this effect.

Once we established the properties of the ferrofluid we measured the mean unbinding force using a magnetic force ramp. For our experiments, we constructed a glass fluid cell in which the substrate surface (initially on top in the fluid cell) was coated either with PEG (Microsurfaces, Austin, TX) or a fluorocarbon that was deposited by vaporization of perfluorooctyltriethylsilyl silane (Alfa Aesar, Ward Hill, MA) onto oxygen plasma cleaned glass slides that were stored in a dessicator until use. A suspension containing 3.2% ferrofluid particles and 0.2% beads by volume was inserted into the fluid cell. Since the beads were less dense than the ferrofluid, they migrated to the top of the fluid cell, where they were allowed to bind to the surface for 25 min. The fluid cell was then inverted, causing any beads that were not adhered to the surface to float away from the focal plane. A 10 min period was sufficient to remove all nonadhered beads.

The force loading experiments were conducted by increasing the magnetic field with square root time dependence to simulate a linear force ramp according to eq 1. We used video tracking and image software analysis to determine the number of beads unbinding from the surface at each frame, which enabled the construction of a histogram to determine the most probable force using a log-normal probability distribution fit (Figure 3a). An unbinding event was identified as the time, and hence magnetic force, at which the bead's fluorescent intensity suddenly decreased, as it was pushed away from the substrate (see Supporting Information Figure 5). In each experiment, we identified several hundred unbinding events to ensure good statistics. Several trials were conducted for each magnetic field ramp to determine the relationship between force loading rate and the most probable unbinding force. Thermally induced fluid flow or other convective forces appeared to be negligible because after an unbinding event, the beads did not experience significant lateral translational motion. We also performed control experiments without a magnetic field and found that less than 5% of the surface-adhered beads were unbound under the action of gravity for time scales in excess of 1 h. This result indicates that data from our unbinding experiments was predominantly unaffected by the offset due to gravity.

At very low loading rates (<0.02 pN/s), the unbinding force is independent of the loading rate (Figure 3b,c), which implies that unbinding likely occurs at quasi-equilibrium conditions. The lowest force loading rate we tested is 1–2 orders of magnitude lower than any other that were previously reported for linear force ramps.⁹ These remarkably low loading rates provided by our magnetic tweezer approach are possible because of the lack of heating and/or mechanical contact with the bead. In other

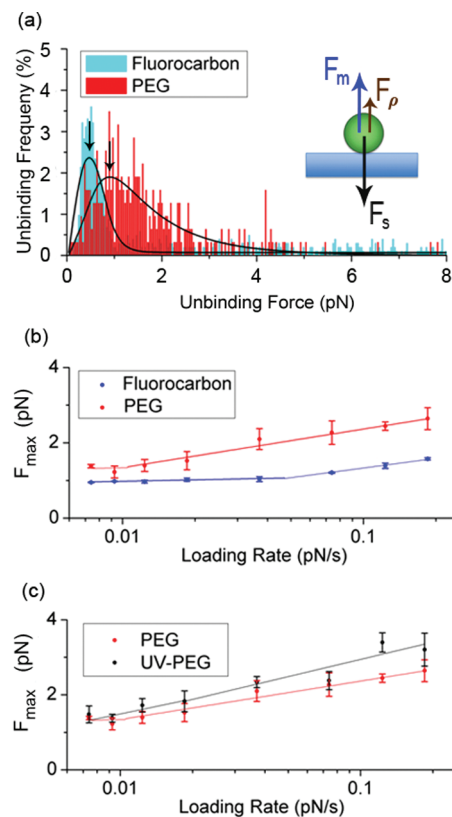


Figure 3. Unbinding histograms and loading rate dependence. Example histograms for PEG (red) and Teflon (cyan) substrates are provided in (a) for 0.0074 pN/s loading rate. The most probable unbinding force, labeled F_{max} , is depicted as a function of the loading rate for (b) Teflon substrates and PEG substrates, and (c) PEG substrates and UV-irradiated PEG substrates.

approaches, including AFM, optical tweezers, and biomembrane force probes, force loading rates are limited to the ranges 10^1 – 10^7 , 10^{-1} – 10^2 , and 10^{-1} – 10^5 pN/s, respectively, due to issues of low-frequency drift of the optical or mechanical components. The equilibrium unbinding force for the fluorocarbon and PEG substrate is the sum of the magnetic force and buoyancy force, which were determined to be 0.974 and 1.339 pN, respectively (Figure 3b). At higher loading rates, the unbinding force depended exponentially on the loading rate, which is consistent with prior studies on the loading rate dependence of intermolecular forces.²¹

The magnetic image force method allows for determination of even small differences in the adhesion properties of surfaces. For example, the mean unbinding force of PEG substrates that were previously irradiated with 254 nm UV radiation (Migge, Heidelberg, Germany) with total energy exposure of 500 kJ/m^2 in air was measured and compared with that from the nonirradiated samples (Figure 3c). Our results showed a slightly larger unbinding force at low loading rates for the UV treated PEG surfaces. In contrast, water contact angle measurements on these surfaces could not detect a difference in surface energy. To our knowledge, this is the first mechanical force-based measurement demonstrating the damaging effects of UV radiation on the surface energetic properties (i.e., adhesion) of PEG surfaces.

The ability of the magnetic tweezer approach to directly measure van der Waals (VdW) surface forces was analyzed^{22,23}

by considering the VdW force between a sphere and half-plane, which scales according to $F_{\text{VdW}} = Ad/12\Delta^2$, where A , the Hamaker constant, depends on the fluid, bead, and substrate electromagnetic properties. The two parameters, A and Δ are not known a priori, and thus some assumptions are required to explain the force data. An estimate for the Hamaker constant neglecting retardation effects can be obtained from the relation²⁴

$$A \approx \frac{3}{4}k_{\text{B}}T \left(\frac{\epsilon_{\text{p}} - \epsilon_{\text{f}}}{\epsilon_{\text{p}} + \epsilon_{\text{f}}} \right) \left(\frac{\epsilon_{\text{s}} - \epsilon_{\text{f}}}{\epsilon_{\text{s}} + \epsilon_{\text{f}}} \right) \quad (3)$$

where ϵ_{p} , ϵ_{f} , and ϵ_{s} are the dielectric constants of the bead, fluid, and substrate, respectively. According to eq 3, when $\epsilon_{\text{f}} \gg (\epsilon_{\text{p}}, \epsilon_{\text{s}})$ the Hamaker constant approaches a constant value of $A \approx 3k_{\text{B}}T/4$, which gives a predicted force that is more than 1000 times greater (assuming physical contact, $\Delta \sim 1$ nm) than what we measured in the quasi-equilibrium regime. Explaining why the experimentally measured VdW force is so low requires the assumption that the bead and surface were separated by a much greater distance ($\Delta \approx 50$ nm). To determine the source of this unexpectedly large bead/substrate separation distance, we used AFM to image the top surface of a bead that was previously immersed in ferrofluid. The adhesion of magnetic nanoparticles onto polystyrene beads has been noted in our prior work,²⁵ and here we show that the ensuing roughness of a magnetic nanoparticle surface layer can explain the magnitude of the measured surface forces (see AFM and scanning electron microscopy (SEM) images in Supporting Information).

There are other surface forces that contribute to the forces measured in our approach, including volume depletion attraction, electrostatic double layer repulsion, and hydrophobic interactions; however we expect these to be quite small in comparison to the VdW force. Because of the large size disparity between the bead and the nanoparticles, the volume depletion attraction is negligibly small.²⁶ The double layer repulsion should also be quite small since the ferrofluid contains an ionic surfactant which significantly reduces the Debye length. Hydrophobic effects also do not appear to be significant since one of the substrates is hydrophilic (PEG) while the other is hydrophobic (fluorocarbon), yet very similar force data was obtained. One could also argue that nanoparticle concentration gradients or other geometric boundary effects could alter the force calculations. In our prior work, we have analyzed the structure of ferrofluid in the presence of field gradients;²⁰ however for the low fields at which these unbinding events typically occurred (~ 20 Oe), the local variation in particle concentration is expected to be small ($< 5\%$). Finally, the image dipole approximation is also known to be inaccurate when the bead/surface separation distances become exceedingly small (less than 1/100th of a diameter). To estimate this effect, we conducted exact calculations in the bispherical coordinate system¹⁶ which suggest that the repulsive force increases by only a very small amount ($\sim 10\%$) when the bead approaches surface contact (see calculations in Supporting Information).

In conclusion, we developed a new technique for simultaneously measuring the adhesion force between thousands of beads and a surface under identical experimental conditions, allowing for the determination of a statistical distribution of surface force measurements in one single experiment. This technique can measure exceedingly small forces with potentially sub-femtoNewton ($< 10^{-15}$ N) resolution if smaller beads are used, making it suitable for a broad range of colloidal surface force

analyses, such as those required to determine bioadhesion and receptor–ligand interactions. Additionally, the ability to measure extremely low force loading rates gives access to quasi-equilibrium force loading regimes, which can match the conditions in some biological systems where the force loading rates are on the time scale of minutes and longer. The availability of a convenient tool for surface force analysis can potentially accelerate the screening and understanding of ligand-protein binding and other biological interactions,²⁷ as well as the development of nonfouling surfaces for various microdevices and implants.²⁸

■ ASSOCIATED CONTENT

S Supporting Information. Additional information and figures. This material is available free of charge via the Internet at <http://pubs.acs.org>.

■ ACKNOWLEDGMENT

The authors are thankful for support from the National Science Foundation CMMI 0625480.

■ REFERENCES

- (1) Greenleaf, W. J.; et al. *Annu. Rev. Biophys. Biomol. Struct.* **2007**, *36*, 171.
- (2) Neuman, K. C.; Nagy, A. *Nat. Methods* **2008**, *5*, 491.
- (3) Burham, N. A.; et al. *Phys. Rev. Lett.* **1990**, *64*, 1931.
- (4) Lo, Y. S.; Zhu, Y. J.; Beebe, T. P. *Langmuir* **2001**, *17*, 3741.
- (5) Neuert, G.; Albrecht, C. H.; Gaub, H. E. *Biophys. J.* **2007**, *93*, 1215.
- (6) Ota, T.; Sugiura, T.; Kawata, S. *Appl. Phys. Lett.* **2005**, *87*, No. 043901.
- (7) Nishizaka, T.; et al. *Nature* **1995**, *377*, 251.
- (8) Wen, J.; et al. *Biophys. J.* **2007**, *92*, 2996.
- (9) Evans, E.; Ritchie, K.; Merkel, R. *Biophys. J.* **1995**, *68*, 2580.
- (10) Evans, E. *Biophys. Chem.* **1999**, *82*, 83.
- (11) Idziak, S. H. J.; et al. *Science* **1994**, *264*, 1915.
- (12) Harris, S. A.; Sands, Z. A.; Laughton, C. A. *Biophys. J.* **2005**, *88*, 1684.
- (13) Assi, F.; et al. *J. Appl. Phys.* **2002**, *92*, 5584.
- (14) Danilowicz, C.; Greenfield, D.; Prentiss, M. *Anal. Chem.* **2005**, *77*, 3023.
- (15) Shang, H.; Lee, G. U. *J. Am. Chem. Soc.* **2007**, *129*, 6640.
- (16) Erb, R. M.; Yellen, B. B. *IEEE Trans. Magn.* **2006**, *42*, 3554.
- (17) Panofsky, W. K. H.; Phillips, M. *Classical Electricity and Magnetism*; Dover: New York, 1962; pp 49–53, 84–86.
- (18) Rosenzweig, R. E. *Ferrohydrodynamics*; Cambridge: New York, 1985; pp 57–59.
- (19) Islam, M. F.; et al. *Phys. Rev. E* **2003**, *67*, No. 021402.
- (20) Erb, R. M.; et al. *J. Appl. Phys.* **2008**, *103*, No. 063916.
- (21) Merkel, R.; et al. *Nature* **1999**, *397*, 50.
- (22) Israelachvili, J. N.; Pashley, R. M. *J. Colloid Interface Sci.* **1984**, *98*, 500.
- (23) Gady, B.; et al. *Phys. Rev. B* **1996**, *53*, 8065.
- (24) Butt, H. J.; Graf, K.; Kappl, M. *Wiley-VCH: Weinheim*, 2003; p 89.
- (25) Erb, R. M.; et al. *Nature* **2009**, *457*, 999.
- (26) Asakura, S.; Oosawa, F. *J. Polym. Sci.* **1958**, *33*, 183.
- (27) Neinhuis, G. U. *Protein/Ligand Interactions: Methods and Applications (Methods in Molecular Biology)*; Humana Press: Totowa, New Jersey, 2005.
- (28) Ma, H.; Hyun, J.; Stiller, P.; Chilkoti, A. *Adv. Mater.* **2004**, *16*, 338.